Iron-Clad Fibers: A Metal-Based Biological Strategy for Hard Flexible Coatings

Matthew J. Harrington, *et al.*

Science **328**, 216 (2010);
DOI: 10.1126/science.1181044

Science (print ISSN 0036-8075; online ISSN 1095-9203) is published weekly, except the last week in December, by the American Association for the Advancement of Science, 1200 New York Avenue NW, Washington, DC 20005.

with T at a steeper rate than the measurement result (Fig. 4). In comparison, at the lower limit of $K_{LATA} = 0$, $K_{ZA} = 0.73$ N/m, and $s = d = 30$ nm, the BTE solution obtains a $\kappa - T$ curve in good agreement with the measurement (Fig. 4). In this case, the ZA contribution to κ becomes smaller than the corresponding TA and LA contributions (*13*), which are reduced only by the suppression of the ZA + ZA → LA or TA mode conversions because of leakage of ZA phonons.

In 2D and at the low T limit, if the scattering rate τ_j^{-1} is proportional to ω^{α}, the κ contribution is proportional to $T^{2-\alpha}$ for j = TA, LA, or ZA polarization. For $K_{LATA} = K_{ZA} = 0.46$ N/m, τ_j^{-1} of all the three polarizations is dominated by $\tau_{sub,j}^{-1}$, for which the α exponent is negative and results in an increased κ with T. In comparison, for $K_{LATA} = 0$ and $K_{ZA} = 0.73$ N/m, boundary scattering with $\alpha = 0$ and isotope and umklapp scatterings with positive α exponents play an increased role for the dominant in-plane polarizations at low and intermediate T, respectively, so that the calculated $\kappa - T$ slope in this T range is relatively small, in agreement with the measured data. On the other hand, we have also fit the measured κ at 300 K by including substrate scattering of $K_{LATA} = 0.8$ N/m in the RTA model (*18*) that neglects the ZA contribution (*13*). The as-calculated κ increases with T at a much more rapid rate than both the BTE results and the experimental data (Fig. 4), because of the negative α exponent of the dominant substrate scattering rate for the LA and TA phonons and the high zone-boundary frequencies of these two branches.

The theoretical analysis suggests that the ZA contribution to κ is large in suspended SLG and that the measured $\kappa - T$ relation can be explained by much stronger substrate scattering of ZA phonons than LA and TA phonons. Although the strong ZA scattering can be caused by the expected behavior of $K_{ZA} > K_{LATA}$, another possibility is that umklapp scattering of ZA phonons can be enhanced by the substrate interaction, which breaks the reflection symmetry. Indeed, our calculations show that the ZA contribution is reduced in suspended bilayer graphene because of interlayer interactions. Although future theoretical work is needed to clarify this issue, our experimental results clearly show that graphene exfoliated on SiO_2 still conducts heat rather efficiently despite phonon-substrate interaction. However, the substrate effect could be quite different for few-layer graphene or SLG grown by thermal decomposition (*27*) or chemical vapor deposition (*28*, *29*) on other substrates because of different interface interactions. These intriguing questions are expected to stimulate further experimental and theoretical investigations of phonon transport in suspended, supported, and embedded graphene.

References and Notes

1. K. S. Novoselov *et al.*, *Science* **306**, 666 (2004).
2. K. I. Bolotin *et al.*, *Solid State Commun.* **146**, 351 (2008).
3. C. Lee, X. Wei, J. W. Kysar, J. Hone, *Science* **321**, 385 (2008).
4. G. A. Slack, *J. Appl. Phys.* **35**, 3460 (1964).
5. G. A. Slack, *Phys. Rev.* **127**, 694 (1962).
6. P. Kim, L. Shi, A. Majumdar, P. L. McEuen, *Phys. Rev. Lett.* **87**, 215502 (2001).
7. C. Yu, L. Shi, Z. Yao, D. Li, A. Majumdar, *Nano Lett.* **5**, 1842 (2005).
8. E. Pop *et al.*, *Phys. Rev. Lett.* **95**, 155505 (2005).
9. Y. S. Ju, K. E. Goodson, *Appl. Phys. Lett.* **74**, 3005 (1999).
10. Y. Yang, W. Liu, M. Asheghi, *Appl. Phys. Lett.* **84**, 3121 (2004).
11. A. A. Balandin *et al.*, *Nano Lett.* **8**, 902 (2008).
12. J. H. Chen, C. Jang, S. Xiao, M. Ishigami, M. S. Fuhrer, *Nat. Nanotechnol.* **3**, 206 (2008).
13. Materials and methods are available as supporting materials on *Science* Online.
14. L. M. Malard, M. A. Pimenta, G. Dresselhaus, M. S. Dresselhaus, *Phys. Rep.* **473**, 51 (2009).
15. E. H. Hwang, E. Rossi, S. Das Sarma, *Phys. Rev. B* **80**, 235415 (2009).
16. Y.-W. Tan *et al.*, *Phys. Rev. Lett.* **99**, 246803 (2007).
17. P. G. Klemens, *Int. J. Thermophys.* **22**, 265 (2001).
18. D. L. Nika, S. Ghosh, E. P. Pokatilov, A. A. Balandin, *Appl. Phys. Lett.* **94**, 203103 (2009).
19. P. G. Klemens, D. F. Pedraza, *Carbon* **32**, 735 (1994).
20. D. L. Nika, E. P. Pokatilov, A. S. Askerov, A. A. Balandin, *Phys. Rev. B* **79**, 155413 (2009).
21. E. Mariani, F. von Oppen, *Phys. Rev. Lett.* **100**, 076801 (2008).
22. L. Lindsay, D. A. Broido, N. Mingo, *Phys. Rev. B* **80**, 125407 (2009).
23. M. Ishigami, J. H. Chen, W. G. Cullen, M. S. Fuhrer, E. D. Williams, *Nano Lett.* **7**, 1643 (2007).
24. V. Geringer *et al.*, *Phys. Rev. Lett.* **102**, 076102 (2009).
25. R. Prasher, *Appl. Phys. Lett.* **94**, 041905 (2009).
26. M. T. Dove, *Introduction to Lattice Dynamics, Cambridge Topics in Mineral Physics and Chemistry 4* (Cambridge Univ. Press, Cambridge, New York, 1993), pp. 29–32.
27. C. Berger *et al.*, *J. Phys. Chem. B* **108**, 19912 (2004).
28. K. S. Kim *et al.*, *Nature* **457**, 706 (2009).
29. X. Li *et al.*, *Science* **324**, 1312 (2009).

30. This work is supported in part by National Science Foundation awards CBET-0553649 and 0933454 (J.H.S. and L.S.), CBET 0651381 (D.A.B. and L.L.), 0651310 (N.M.), and CMMI-0926851 (Z.H.A. and R.H.); Office of Naval Research award N00014-08-1-1168 (A.L.M. and L.S.); Department of Energy Office of Science award DE-FG02-07ER46377(M.T.P. and L.S.); and The University of Texas at Austin (R.S.R.).

Supporting Online Material

www.sciencemag.org/cgi/content/full/328/5975/213/DC1
SOM Text
Figs. S1 to S11
References

30 October 2009; accepted 24 February 2010
10.1126/science.1184014

Iron-Clad Fibers: A Metal-Based Biological Strategy for Hard Flexible Coatings

Matthew J. Harrington,[1]*† Admir Masic,[1]† Niels Holten-Andersen,[2,3] J. Herbert Waite,[2,4] Peter Fratzl[1]

The extensible byssal threads of marine mussels are shielded from abrasion in wave-swept habitats by an outer cuticle that is largely proteinaceous and approximately fivefold harder than the thread core. Threads from several species exhibit granular cuticles containing a protein that is rich in the catecholic amino acid 3,4-dihydroxyphenylalanine (dopa) as well as inorganic ions, notably Fe^{3+}. Granular cuticles exhibit a remarkable combination of high hardness and high extensibility. We explored byssus cuticle chemistry by means of in situ resonance Raman spectroscopy and demonstrated that the cuticle is a polymeric scaffold stabilized by catecholato-iron chelate complexes having an unusual clustered distribution. Consistent with byssal cuticle chemistry and mechanics, we present a model in which dense cross-linking in the granules provides hardness, whereas the less cross-linked matrix provides extensibility.

Metal complexation in biological and bioengineered load-bearing structures is emerging as a versatile cross-linking strategy for assembling and mechanically reinforcing polymeric materials (*1*–*6*). Coordination complexes form cross-links when two or more ligands each donate a nonbonding electron pair to empty orbitals in a transition metal ion. Because of their high stability and rates of formation (*7*–*9*), coordination-based cross-links have been proposed to endow certain biological structures with a number of desirable material properties, including triggered self-assembly, increased toughness, self-repair, adhesion, high hardness in the absence of mineralization, and mechanical tunability (*1*–*4*, *7*). Spectroscopic evidence for the presence of coordination complexes in these various materials is often quite compelling (*10*, *11*), and the loss of material stiffness and hardness upon metal removal is strongly suggestive of a cross-linking role (*1*, *2*, *12*, *13*). Precise localization of coordination complexes in situ has remained elusive but is essential in

[1]Department of Biomaterials, Max Planck Institute for Colloids and Interfaces, Potsdam 14424, Germany. [2]Biomolecular Science and Engineering, University of California, Santa Barbara (UCSB), Santa Barbara, CA 93106, USA. [3]Department of Chemistry, University of Chicago, Chicago, IL 60637, USA. [4]Department of Molecular, Cellular, and Developmental Biology, UCSB, Santa Barbara, CA 93106, USA.

*To whom correspondence should be addressed. E-mail: Matt.Harrington@mpikg.mpg.de
†These authors contributed equally to this work.

defining structure-function relations. Here, we report on the precise localization of metal-protein complexes in mussel byssus by use of Raman microscopy.

The byssus, a shock-absorbing fibrous holdfast made by marine mussels (Fig. 1A), is a treasure trove of metal-polymer complexes, making it a suitable model system for investigating the load-bearing properties of metal coordination cross-links (*3*, *4*, *10*, *13*). Mussels use the byssus, a bundle of 50 to 100 individual threads that are extensible up to >100% strain, to fasten themselves to accessible surfaces of the rocky seashore (Fig. 1A) (*14*). Threads are formed one at a time by a secretion of soluble precursors (primarily protein) into a narrow groove of the thread-forming organ known as the foot. After assembly of the fibrous interior, a 2- to 5–μm-thick protective cuticle is applied as a separate secretion (Fig. 1, B and C) (*15*). Mechanically, the cuticle exhibits a hardness four- to fivefold higher than the fibrous core while maintaining, depending on the species, a breaking strain as high as 100% (Fig. 1B) (*16*, *17*). High cuticle failure strains are correlated with the presence of interspersed granules (Fig. 1C) that hinder crack propagation at high strains via the formation of numerous dispersed microcracks within the continuous intergranular matrix (*16*, *17*). Traditional engineering coatings with comparable hardness fail catastrophically long before reaching such strains.

Mussel foot protein 1 (mfp-1) is the only protein known to be present in the cuticle and is characterized by a high isoelectric point (pI) (~10), minimal secondary structure, and on average 10 to 15 mole percent (mol %) of a posttranslational modification of tyrosine known as 3,4-dihydroxyphenylalanine (dopa) (*18*–*20*). Mfp-1 consists largely of a tandemly repeated decapeptide $x_1Lys_2x_3x_4Tyr_5x_6x_7x_8Tyr_9Lys_{10}$, in which $Lys_{2,10}$ and $Tyr_{5,9}$ are completely conserved and the differential hydroxylation of tyrosine to dopa leads to the accumulation of two mfp-1 populations: (i) one with dopa limited to Tyr_9 and (ii) another with dopa at both Tyr_5 and Tyr_9 (*21*). The inorganic cuticle component, which comprises ~1% of the dry weight, includes metal ions, particularly iron and calcium, but mineralization is absent (*13*). The colocalization of Fe and dopa in the cuticle combined with the unusually high stability of catecholato-Fe^{3+} complexes has led to the proposition that dopa-Fe complexes provide cross-links between mfp-1 chains (Fig. 1D) (*10*, *13*, *22*–*24*). Taylor *et al.* (*23*) demonstrated the ability of mfp-1 to bind Fe^{3+} ions via dopa ligands in vitro using resonance Raman spectroscopy; however, dopa-metal cross-links have not been detected within the cuticle. We investigated the presence and distribution of dopa-dependent metal coordination within the cuticle in situ by exploiting the sub-micrometer resolution of confocal Raman spectroscopy. Results offer revealing insights into the spatial organization of dopa-Fe complexes in the cuticle and support an integral role of metal coordination chemistry in mechanical performance.

The resonance Raman spectra of *Mytilus californianus* and *M. galloprovincialis* thread cuticles are nearly identical (Fig. 2A) despite slight differences in the primary sequence of their respective mfp-1s and the average granule size (*M. californianus*, 200 ± 80 nm; *M. galloprovincialis*, 750 ± 200 nm) (*17*). Nearly all peaks can be attributed to the resonance enhanced interaction of iron (or a related transition-metal ion) with the catecholic moiety of dopa (Fig. 2A and table S1) (*23*, *25*). The peaks at 550, 596, and 637 cm^{-1} are assigned specifically to bidentate chelation of the metal ion by the phenolic oxygens of dopa and will be used throughout as an indicator of the presence of dopa-metal complexation (*26*). The peak at 415 cm^{-1} did not appear in previous in vitro spectra of mfp-1–Fe^{3+} solutions and therefore could not be confidently assigned (*23*); however, possible assignments based on similar chemical systems, particularly didopa cross-linking, are discussed in the supporting online material (SOM) text (table S2). The resonance Raman spectra are stable and persist in cuticles even after 15 days in raw seawater (fig. S1). There were no observable changes in the spectra of the cuticle during or after tensile strains of 100% (SOM text).

The specific enhancement of resonance peaks allows us to localize sites of dopa-metal coordination within the thread. Raman spectroscopic imaging was performed on freshly cut transverse cross-sections of *M. californianus* threads, and peak distribution maps were generated by the integration of the intensity of specific assigned peaks (Fig. 2B). The region corresponding to aliphatic CH vibrations, which is not resonance-dependent, is evenly distributed between the coating and core of the thread, indicating a constant distribution of organic material. In contrast, resonance peaks from catechol-metal interactions and catechol ring vibrations are localized exclusively within the outer cuticle of the thread (Fig. 2B).

It has been previously observed that EDTA depletes iron and calcium ions in the cuticle and results in a ~50% reduction in hardness of the material (*13*). Consistent with this observation, Raman spectra from EDTA-treated thread cuticles show a nearly complete loss of the metal-associated resonance peaks (Fig. 2C). When EDTA-treated threads are then soaked in a 1-mM solution of $FeCl_3$ for 1 hour, catechol-metal resonance is largely recovered; spectral differences between native and treated cuticles are minor (Fig. 2C). The most striking difference is the disappearance of the 415 cm^{-1} peak and the appearance of a group of peaks centered around 330 cm^{-1}. Treatment with $FeCl_3$ alone was sufficient to regenerate spectra; inclusion of $CaCl_2$ in the solution was not necessary.

Mytilus byssus cuticle is not a homogenous structure; rather, it resembles a particle-reinforced composite (Fig. 1C). To further investigate dopa-metal complex distribution within the composite cuticle, microtomed thin sections of *M. galloprovincialis* threads were prepared and imaged with Raman spectroscopy. Light microscopy of cuticle sections (with thicknesses of ~3 μm) revealed a dark granular consistency (Fig. 3A). A two-dimensional (2D) Raman image of the same region integrated for the catechol-metal resonance peak shows that the granular inclusions seen in Fig. 3A appear as regions of high signal intensity and that the matrix shows a weak but measurable

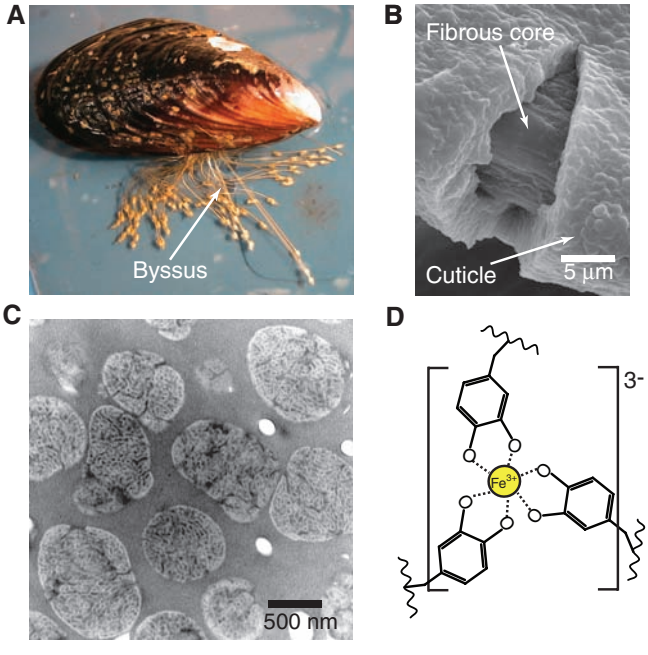

Fig. 1. Mussel byssus cuticle. (**A**) Mussels produce a byssus composed of numerous extensible, shock-absorbing byssal threads. Threads are made one at a time by the mussel foot and attached to hard surfaces by adhesive plaques. (**B**) Mytilid threads are covered by a thin (~5 μm) cuticle with a granular morphology. Strain-induced macrotearing of cuticle exposing the underlying fibrous core is evident in the SEM. The onset of macroscopic cuticle failure in some species requires strains as high as 70 to 100% despite the four- to fivefold greater hardness of cuticle vis-à-vis the extensible interior. (**C**) Granular microstructure as revealed by means of transmission electron microscopy (TEM) in an osmium-stained cuticle. (**D**) The hexadentate mononuclear tris dopa-iron coordination complex proposed to cross-link mfp-1 in the byssus coating.

signal (Fig. 3B). To further verify that the distribution of dopa-metal signal stems from variation in sample composition and not topography or thickness, a depth scan (in the *z* plane) was performed across a region in which the granules were particularly well-resolved, confirming that granules are regions of high intrinsic signal intensity (Fig. 3C). Analysis of the region within the highlighted box in Fig. 3C indicates that the maximum granule and minimum matrix intensities of the integrated catechol-metal peak differ by a factor of ~2 to 3.

From these data, we infer that the granules contain a higher dopa-metal cross-link density than the surrounding matrix. By extension, a reasonable prediction would be that the mechanical behavior of the granules differs from that of the matrix. Previous atomic force microscopy (AFM)–based studies have shown that during elongation of *M. galloprovincialis* cuticle, the granule aspect ratio increases up to ~30% in proportion to cuticle strain, indicating that the matrix and granules behave essentially as a single phase (*16*). However, above ~30% strain the granules essentially stop deforming, shifting further strain to the surrounding matrix (*16*). Microcrack formation is consequently observed in the cuticle, but not within the granules (*16*). Furthermore, by returning stretched threads (50% strain) to their initial length and then immediately measuring aspect ratios, we observed that whereas granule elongation is instantaneously reversible, recovery from microcracks is not (Fig. 3D and fig. S3). Cuticle microcracking qualitatively resembles the large-scale cavitation observed in synthetic nanocomposites in which hard inclusions are embedded in a softer polymer (*27*), suggesting that past 30% strain granules behave more stiffly and are less compliant than the matrix.

Several findings of this study point toward a key role of metal cross-links within the cuticle polymer: (i) Cuticle cohesion is based on the presence of dopa-metal cross-links. (ii) The non-covalent and reversible nature of this bonding structure, evident from EDTA and $FeCl_3$ recovery experiments, demonstrates its inherent versatility as compared with that of covalent cross-links (Fig. 2C). (iii) In light of previous nanoindentation-based studies (*13*), the results of EDTA treatment strongly support the role that dopa-iron cross-linking plays in modulating cuticle mechanical properties. And (iv), granules were shown to have a higher relative resonance signal than the matrix, which is indicative of a higher density of dopa-metal–based cross-linking within the granules.

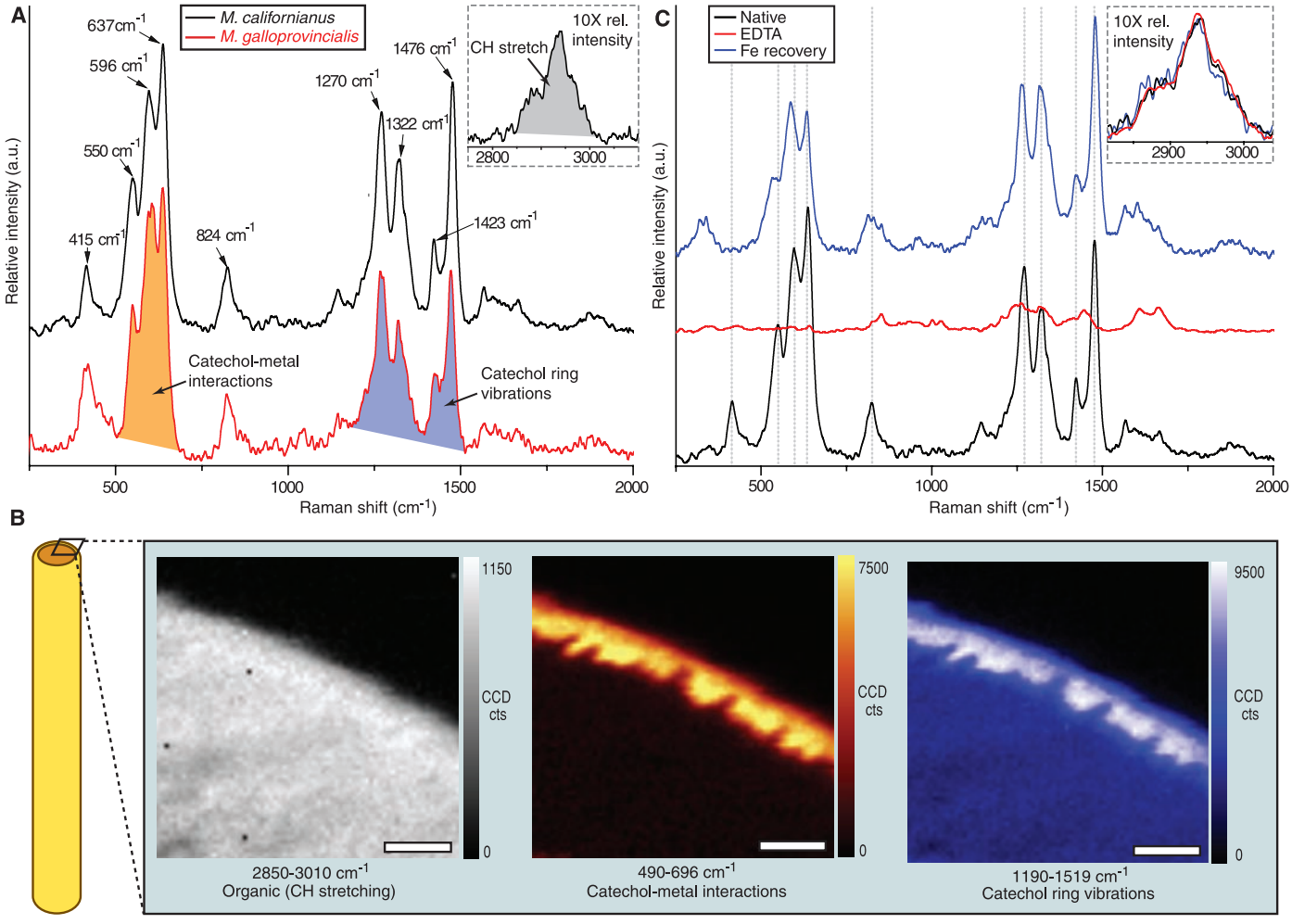

Fig. 2. Raman spectroscopy of byssus cuticles. (**A**) Resonance Raman spectra from *M. californianus* and *M. galloprovincialis* cuticles. The cuticle spectra correspond closely to spectra of mefp-1 and Fe^{3+} in vitro (*23*). Despite differences in cuticle morphology and mfp-1 sequence in the two species, the spectra are barely distinguishable. (Inset) The nonresonance peak for aliphatic CH stretching from *M. californianus* cuticle magnified 10× the relative intensity. According to the assignments, the most prominent peaks can be attributed to the interaction of metal with the catecholic oxygens and to the vibrations of the carbon bonds in the catechol ring, respectively. (**B**) 2D Raman imaging of the same transverse *M. californianus* thread section integrated over three different wave-number ranges as indicated. Organic material is uniformly distributed; however, dopa-Fe^{3+} resonance is confined to the outer coating. Scale bars, 5 μm. (**C**) Resonance Raman spectra of thread cuticles from *M. californianus* in the native state, after EDTA treatment, and after re-exposure to Fe in a depleted thread. The nearly complete loss of resonance peaks after EDTA treatment is reversed by a nearly complete restoration by means of incubation in 1 mM $FeCl_3$ (pH3.2). The three spectra were normalized to the area under the aliphatic CH peak [2850 to 3010 cm^{-1} (inset)].

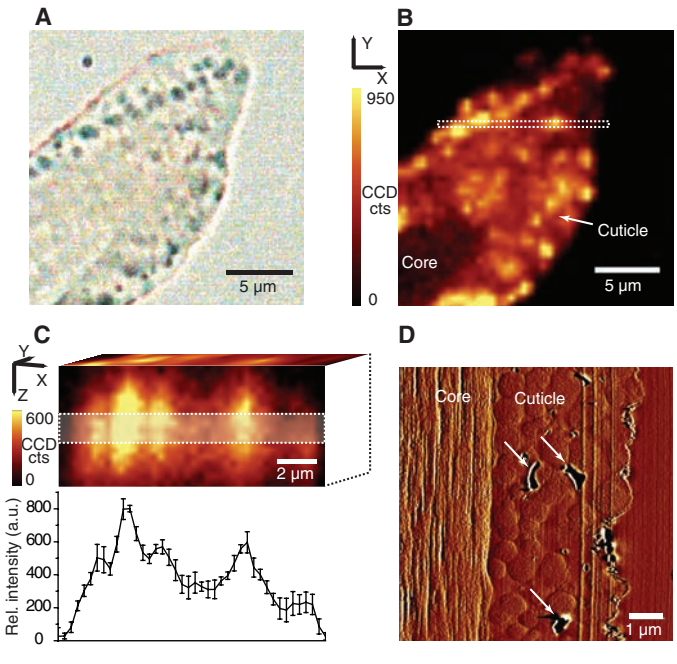

Fig. 3. High-resolution Raman imaging of byssus cuticle. (**A**) Light micrograph of a thin section (~3 μm) of *M. galloprovincialis* proximal cuticle with granules evident as dark spots (100× oil immersion). (**B**) 2D Raman image of (A) integrated for the Fe-catechol peak (490 to 696 cm^{-1}) reveals that granules have higher intensity than matrix. (**C**) Raman depth scan along trajectory (dashed box) in (B) further accentuates the strong difference in the Raman resonance signal between the granules and the matrix. The elongated shape of the granules in the *z* axis is an artifact resulting from the vertical resolution limit of the confocal Raman microscope. The relative intensity (mean ± SD) at each point along the *x* axis averaged over the height (*z* axis) of the highlighted box is plotted below the scan. (**D**) AFM amplitude image of a relaxed thread (recovered after 50% strain) showing the recovered shape of the granules and widespread cuticle microcracking (white arrows).

Although amino acid–metal complexes, particularly those involving dopa or histidine as ligands, are less than half as strong as covalent bonds, they are reversibly breakable through hundreds of cycles (*7*, *9*). Two different mechanical roles have been attributed to these cross-links in biological structures. First, in several damage-tolerant biological structures, low densities of metal complexes are believed to function as reversible sacrificial bonds. For instance, the collagenous core of byssal threads, which exhibits remarkable toughness and self-healing, is stabilized by histidine-metal complexes as opposed to typical collagen cross-linking chemistry (*4*). Similarly, spider silk infiltrated with transition metal ions acquires a substantial increase in toughness, probably because of the formation of coordination complexes (*5*). Second, in contrast to this proposed sacrificial role, the high density of histidine-zinc complexes in the jaws of marine worms (*Nereis* sp.) is adapted to fashion a lightweight material as hard as dentin in the absence of a mineral phase (*1*).

Conceivably, the byssus cuticle combines both of these cross-linking strategies to achieve its unique blend of hardness and extensibility. Consider a view of the cuticle as a continuous network of loosely folded mfp-1 chains with

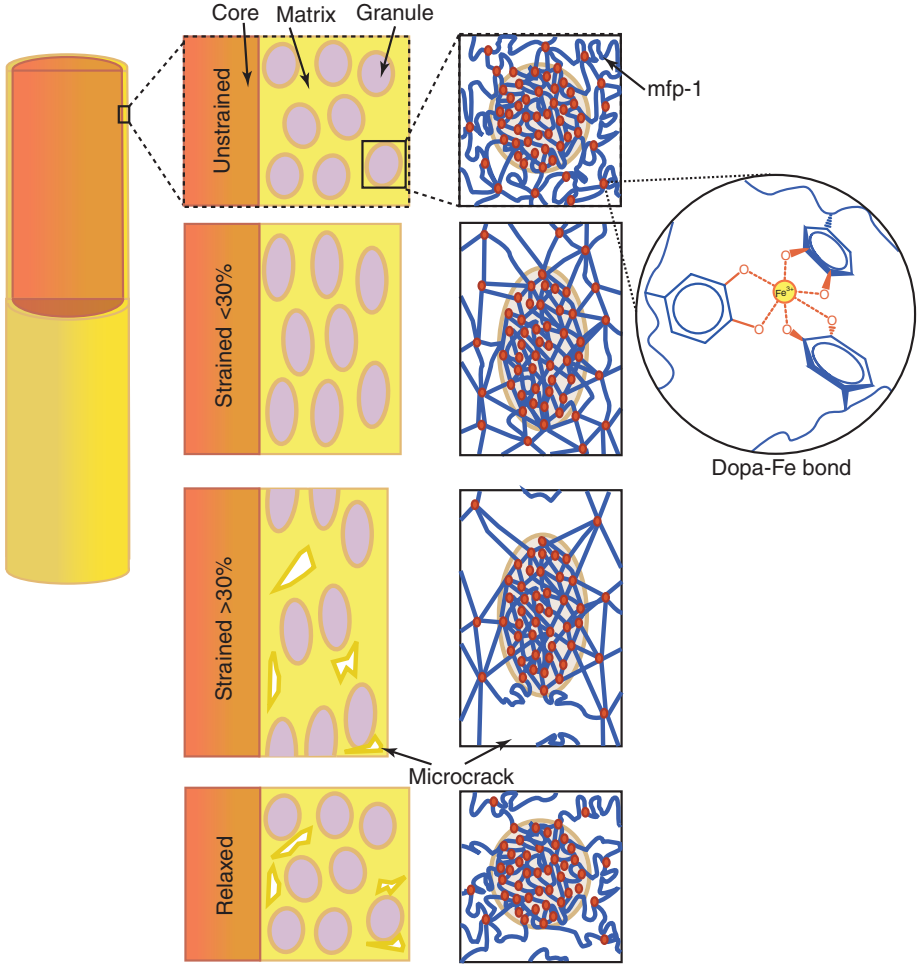

Fig. 4. Basic model illustrating the cohesive role of dopa-Fe complexes in the byssus cuticle. Granules contain a higher cross-link density than matrix. When the cuticle is stretched to less than 30% strain, the randomly coiled mfp-1 chains begin to unravel, and the granule and matrix deform equivalently. However, when stretched beyond 30% strain mfp-1 chains are largely unraveled, and microcracks form outside the granules because of the difference in cross-link density. When relaxed, the granule returns to its initial shape, whereas microcracks do not exhibit immediate recovery.

dopa-metal cross-link density that alternates from high (granules) to low (matrix) (Fig. 4). This model assumes that mfp-1 is the primary structural component of the coating, and although other types of bonding are expected to contribute to the overall stabilization of the structure, we focus here only on the potential role of dopa-Fe cross-linking (*18*). At the onset of cuticle strain, mfp-1 chains [which at rest are random coils and short bent helices (*20*)] straighten out. Within this range, the granules and matrix exhibit similar (high) compliance; however, at ~30% strain most of the coiled protein domains are unraveled, and the load is transferred to the metal-based cross-links. Because of their higher cross-link density, the granules oppose further deformation at the expense of the less cross-linked matrix (Fig. 4). This is perhaps the point at which the lability of dopa-Fe complexes becomes instrumental to cuticle function by facilitating the formation of dispersed microcracks and sparing the cuticle from catastrophic failure. The relatively low forces required to completely unfold noncovalently stabilized random coil domains [~100 pN for the PEVK domain of the muscle protein titin (*28*)] versus those required to break a dopa-metal bond [~800 pN (*7*)] support the sequence of sacrificial bond breakage put forward in this model; however, alternative interpretations should still be considered.

An open question concerns the mechanism of local control over the cross-link density by the organism. There are two plausible explanations: (i) Granules represent a condensed protein phase with higher mfp-1, and consequently dopa density, than the matrix. High-resolution electron micrographs of cuticle-forming cells reveal that secretory vesicles undergo a maturation process that resembles phase separation to form a prefabricated granule surrounded by matrix (*15*). Or (ii), granules have more cross-links per protein chain (for example, mfp-1 within the granules could have more Tyr modified to dopa residues). Two populations of mfp-1 differing only in the degree of dopa modification have been identified (*18*, *21*). It should be added that the two explanations are not mutually exclusive.

The use of dopa-Fe complexes to "ironclad" a polymeric coating is also notable considering the costly cellular processing required. What is the adaptive benefit of forming redox-active dopa by means of posttranslational processing when histidine could be used for metal cross-linking at lower cost? Possibilities include using post-translational modifications to tune cross-link density [as exemplified by the two mfp-1 populations (*21*)], linking dopa-Fe redox exchange to didopa cross-link formation (table S2) (*10*), and exploiting the remarkable affinity of the dopa-Fe^{3+} complex in iron-limited marine environments (SOM text) (*24*, *29*).

This study provides in situ evidence for the peculiar metallopolymeric structures used to stabilize the load-bearing network in the byssus cuticle. In light of previous mechanical studies, these data support the notion that density and organization of metal complexation in functional biopolymers can be fine-tuned for desirable material properties. The adaptive design of the byssal cuticle is unusual in this regard because the density of metal complexation is strategically varied within the polymeric structure at the sub-micrometer scale in order to create a material that is both hard and extensible—an ideal coating for compliant substrates.

References and Notes

1. C. C. Broomell, M. A. Mattoni, F. W. Zok, J. H. Waite, *J. Exp. Biol.* **209**, 3219 (2006).
2. S. W. Werneke, C. Swann, L. A. Farquharson, K. S. Hamilton, A. M. Smith, *J. Exp. Biol.* **210**, 2137 (2007).
3. M. J. Harrington, J. H. Waite, *Biomacromolecules* **9**, 1480 (2008).
4. M. J. Harrington, H. S. Gupta, P. Fratzl, J. H. Waite, *J. Struct. Biol.* **167**, 47 (2009).
5. S. M. Lee *et al.*, *Science* **324**, 488 (2009).
6. M. M. Pires, J. Chmielewski, *J. Am. Chem. Soc.* **131**, 2706 (2009).
7. H. Lee, N. F. Scherer, P. B. Messersmith, *Proc. Natl. Acad. Sci. U.S.A.* **103**, 12999 (2006).
8. Z. S. Zhang, R. B. Jordan, *Inorg. Chem.* **35**, 1571 (1996).
9. L. Schmitt, M. Ludwig, H. E. Gaub, R. Tampé, *Biophys. J.* **78**, 3275 (2000).
10. M. J. Sever, J. T. Weisser, J. Monahan, S. Srinivasan, J. J. Wilker, *Angew. Chem. Int. Ed.* **43**, 448 (2004).
11. H. C. Lichtenegger *et al.*, *Proc. Natl. Acad. Sci. U.S.A.* **100**, 9144 (2003).
12. E. Vaccaro, J. H. Waite, *Biomacromolecules* **2**, 906 (2001).
13. N. Holten-Andersen *et al.*, *Langmuir* **25**, 3323 (2009).
14. E. Carrington, J. Gosline, *Am. Malacol. Bull.* **18**, 135 (2004).
15. L. Vitarello Zuccarello, *Tissue Cell* **13**, 701 (1981).
16. N. Holten-Andersen, G. E. Fantner, S. Hohlbauch, J. H. Waite, F. W. Zok, *Nat. Mater.* **6**, 669 (2007).
17. N. Holten-Andersen, H. Zhao, J. H. Waite, *Biochemistry* **48**, 2752 (2009).
18. C. J. Sun, J. H. Waite, *J. Biol. Chem.* **280**, 39332 (2005).
19. C. V. Benedict, J. H. Waite, *J. Morphol.* **189**, 171 (1986).
20. S. Haemers, M. C. van der Leeden, G. Frens, *Biomaterials* **26**, 1231 (2005).
21. J. H. Waite, T. J. Housley, M. L. Tanzer, *Biochemistry* **24**, 5010 (1985).
22. S. Haemers, M. C. van der Leeden, G. J. M. Koper, G. Frens, *Langmuir* **18**, 4903 (2002).
23. S. W. Taylor, D. B. Chase, M. H. Emptage, M. J. Nelson, J. H. Waite, *Inorg. Chem.* **35**, 7572 (1996).
24. A. Avdeef, S. R. Sofen, T. L. Bregante, K. N. Raymond, *J. Am. Chem. Soc.* **100**, 5362 (1978).
25. L. Öhrström, I. Michaud-Soret, *J. Am. Chem. Soc.* **118**, 3283 (1996).
26. I. Michaud-Soret, K. K. Andersson, L. Que Jr., J. Haavik, *Biochemistry* **34**, 5504 (1995).
27. C. M. Chan, J. S. Wu, J. X. Li, Y. K. Cheung, *Polymer (Guildf.)* **43**, 2981 (2002).
28. H. B. Li *et al.*, *Proc. Natl. Acad. Sci. U.S.A.* **98**, 10682 (2001).
29. S. W. Taylor, G. W. Luther, J. H. Waite, *Inorg. Chem.* **33**, 5819 (1994).

30. L. Bertinetti (University of Torino) provided technical expertise in operating diffuse-reflectance ultraviolet-vis spectrometry. S. Wasko assisted with scanning electron microscopy (SEM). P.F., M.J.H., and A.M. are grateful for support by the Alexander von Humboldt Foundation and the Max Planck Society in the framework of the Max Planck Research Award funded by the Federal Ministry of Education and Research. M.J.H. was partially funded by an Alexander von Humboldt Research Fellowship for Postdoctoral Researchers. J.H.W. was funded by a grant from NIH (R01DE018468). N.H.A. thanks the Danish Natural Science Research Council for a post-doctoral fellowship (272-08-0087). This work made use of the Materials Research Laboratory central facilities at UCSB supported by the Materials Research and Engineering Center Program of NSF under award DMR05-20415.

Supporting Online Material

www.sciencemag.org/cgi/content/full/science.1181044/DC1
Materials and Methods
Figs. S1 to S4
Tables S1 and S2
References

25 August 2009; accepted 28 January 2010
Published online 4 March 2010;
10.1126/science.1181044
Include this information when citing this paper.

Solvent-Mediated Electron Hopping: Long-Range Charge Transfer in $IBr^-(CO_2)$ Photodissociation

Leonid Sheps,[1] Elisa M. Miller,[1] Samantha Horvath,[2] Matthew A. Thompson,[1]* Robert Parson,[1]† Anne B. McCoy,[2]† W. Carl Lineberger[1]†

Chemical bond breaking involves coupled electronic and nuclear dynamics that can take place on multiple electronic surfaces. Here we report a time-resolved experimental and theoretical investigation of nonadiabatic dynamics during photodissociation of a complex of iodine monobromide anion with carbon dioxide [$IBr^-(CO_2)$] on the second excited (A′) electronic state. Previous experimental work showed that the dissociation of bare IBr^- yields only I^- + Br products. However, in $IBr^-(CO_2)$, time-resolved photoelectron spectroscopy reveals that a subset of the dissociating molecules undergoes an electron transfer from iodine to bromine 350 femtoseconds after the initial excitation. Ab initio calculations and molecular dynamics simulations elucidate the mechanism for this charge hop and highlight the crucial role of the carbon dioxide molecule. The charge transfer between two recoiling atoms, assisted by a single solvent-like molecule, provides a notable limiting case of solvent-driven electron transfer over a distance of 7 angstroms.

Chemical transformations involve the coupling of electronic and nuclear motions as reactants evolve into products, and a central goal of chemical physics is to obtain a molecular-level picture of the underlying fundamental rules that govern reaction dynamics. Such detailed understanding requires the knowledge of reactive potential-energy surfaces, and many in-